

## Nickel–Carbene Complexes

## Transition Metal Compounds of Pyridine-Amide-Functionalized Carbene Ligands: Synthesis, Structure, and Electrocatalytic Properties in Proton Reduction

Siyuan Luo,<sup>[a]</sup> Maxime A. Siegler,<sup>[b]</sup> and Elisabeth Bouwman\*<sup>[a]</sup>

**Abstract:** Three pyridyl-amide substituted (benz)imidazolium salts H<sub>2</sub>L1Cl, H<sub>2</sub>L2Cl and H<sub>2</sub>L3Cl were synthesized and successfully employed as ligand precursors for the syntheses of novel nickel(II) and cobalt(III) complexes. The compounds H<sub>2</sub>L1Cl and H<sub>2</sub>L2Cl are precursors to tridentate ligands and differ in the nature of the N-heterocyclic carbene (NHC) functionality, being imidazole-based and benzimidazole-based, respectively. The ligand precursor H<sub>2</sub>L3Cl resembles H<sub>2</sub>L1Cl, but with one of the pyridyl groups replaced with a benzyl group, thus yielding a potential tridentate ligand. The nickel(II) compounds [Ni(L1)]Cl and [Ni(L2)]PF<sub>6</sub> were obtained, bearing tetradentate ligands comprising an amidate and two pyridine nitrogen donor atoms

and an (NHC) carbon donor. Single crystal X-ray crystallography revealed that the nickel ions in both compounds are in slightly distorted square-planar geometries. Reactions of cobalt salts with the ligands H<sub>2</sub>L1Cl and H<sub>2</sub>L3Cl resulted in the cobalt(III) compounds [Co(L1)<sub>2</sub>]Cl and [Co(L3)<sub>2</sub>]PF<sub>6</sub>; the cobalt ions in both complexes are in octahedral geometries, bound by two tridentate ligands in a meridional binding mode, with two dangling pyridine and benzyl groups, respectively. The four compounds show electrocatalytic activity in proton reduction in dimethylformamide solutions in presence of acetic acid; their activity is compared using cyclic voltammetry and quantified with gas chromatography.

## Introduction

Dihydrogen gas is a promising energy carrier and has emerged as a good alternative for fossil fuel resources, which can be used to meet the rapidly increasing global energy demands.<sup>[1]</sup> Aiming to avoid the use of the expensive Pt-based catalyst, the study of the hydrogen evolution reaction (HER) using molecular catalysts based on non-noble metals has received extensive attention in recent decades. The development of an inexpensive catalyst with high stability and operating at low overpotential with high catalytic turnover rates is of great significance. Hydrogenase enzymes act as effective catalysts in the hydrogen evolution reaction at ambient temperatures and pressures. Unfortunately, synthetic molecular catalyst often suffer from decomposition in aqueous acidic media, resulting in the formation of heterogeneous catalyst systems.<sup>[2]</sup>

In the last decade the cobaloxime-type catalysts,<sup>[3]</sup> and nickel-based catalysts with diphosphane ligands<sup>[4]</sup> have been

shown to have high activity in the electrocatalytic proton reduction reaction. Additionally, molecular catalyst based on molybdenum,<sup>[5]</sup> zinc,<sup>[6]</sup> manganese,<sup>[7]</sup> and copper<sup>[8]</sup> have also been reported to have outstanding activities. Our interest is in the development of novel nickel or cobalt-based homogeneous catalysts supported by N-heterocyclic carbene (NHC) ligands.<sup>[9,10]</sup> Such NHC ligands functionalized with pyridine groups have been used to synthesize nickel and palladium complexes that were found to be efficient catalysts for the Kumada cross-coupling<sup>[9–11]</sup> and Heck-type coupling reactions.<sup>[12]</sup> Nevertheless, so far metal-NHC complexes have received little attention regarding their potential electrochemical properties and activity in electrocatalysis.<sup>[13–17]</sup>

Herein, we report the synthesis and characterization of two novel nickel(II) compounds as well as two cobalt(III) complexes supported by tridentate or tetradentate N-functionalized carbene ligands. We report their redox properties and their electrocatalytic activity for proton reduction in dimethylformamide, with the aim to discuss how carbene backbones and pyridyl groups affect the electrocatalytic activity of the complexes in HER.

## Results and Discussion

## Synthesis of Ligand Precursors and Metal-NHC Complexes

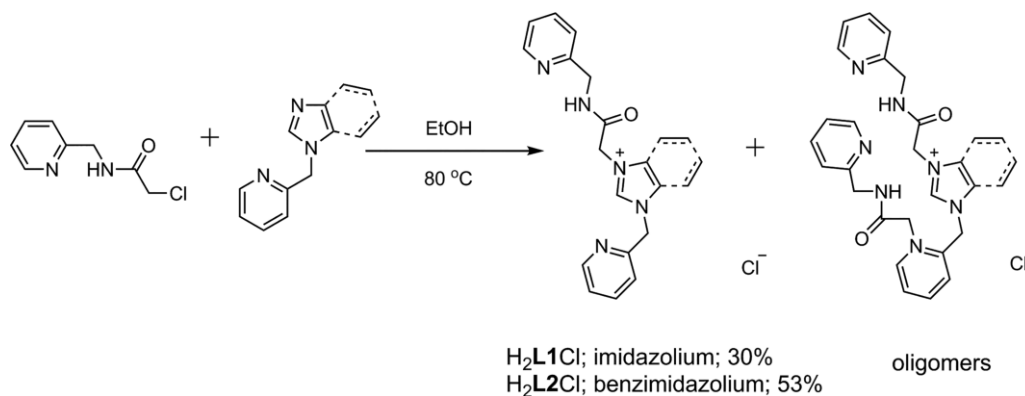
The two new (benz)imidazolium salts H<sub>2</sub>L1Cl and H<sub>2</sub>L2Cl were designed for their use as ligand precursors for the formation of tetradentate anionic NHC ligands, comprising amide and pyrid-

[a] Leiden Institute of Chemistry, Gorlaeus Laboratories, Leiden University, P.O. Box 9502, 2300 RA Leiden, The Netherlands  
E-mail: bouwman@chem.leidenuniv.nl  
<https://www.universiteitleiden.nl/en/science/chemistry/mcbim>

[b] Department of Chemistry, Johns Hopkins University, 3400 N. Charles Street, Baltimore, Maryland 21218, USA

Supporting information and ORCID(s) from the author(s) for this article are available on the WWW under <https://doi.org/10.1002/ejic.201801131>.

© 2018 The Authors. Published by Wiley-VCH Verlag GmbH & Co. KGaA. This is an open access article under the terms of the Creative Commons Attribution-NonCommercial-NoDerivs License, which permits use and distribution in any medium, provided the original work is properly cited, the use is non-commercial and no modifications or adaptations are made.



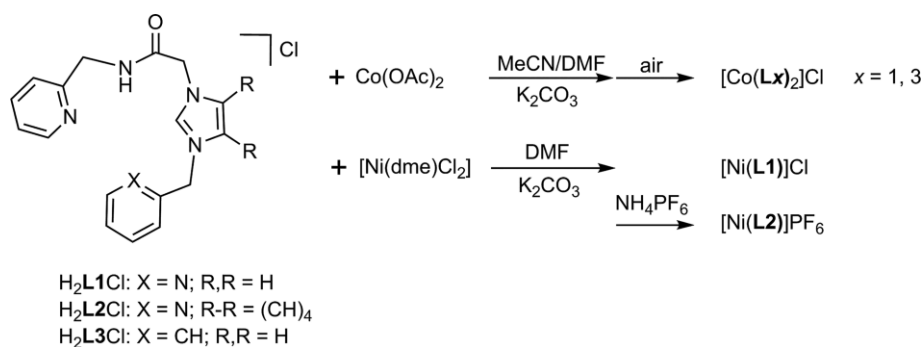
Scheme 1. Synthetic route of the ligand precursors  $\text{H}_2\text{L1Cl}$  and  $\text{H}_2\text{L2Cl}$ .

ine donor moieties. Alkylation of *N*-pyridylmethyl(benz)imidazole appeared to be not straightforward. The relatively high reactivity of the pendant pyridyl group resulted in the formation of oligomeric side products (Scheme 1), giving relatively low yields of the desired products (30 %-50 %). The reported imidazolium salt  $\text{H}_2\text{L3Cl}$  containing a benzyl group was synthesized following a literature procedure.<sup>[18]</sup> The (benz)imidazolium salts were characterized by NMR spectroscopy and electrospray ionization mass spectrometry (ESI-MS). In the  $^1\text{H}$  NMR spectra the characteristic downfield signals for the imidazolium NCHN and amide NH protons were observed at 9.32 and 9.15 ppm for  $\text{H}_2\text{L1Cl}$  and at 10.02 and 9.44 ppm for  $\text{H}_2\text{L2Cl}$ . The ESI-MS spectra exhibited base peaks corresponding to the  $[\text{M} - \text{Cl}]^+$  (benz)imidazolium cations.

Nickel(II) complexes were prepared by reacting the ligand precursors  $\text{H}_2\text{L1Cl}$  and  $\text{H}_2\text{L2Cl}$  with  $[\text{Ni}(\text{dme})\text{Cl}_2]$  in DMF in the presence of  $\text{K}_2\text{CO}_3$  at room temperature and were isolated as yellow solids. The complex  $[\text{Ni}(\text{L1})]\text{Cl}$  was obtained as a pure product after dilution of the reaction mixture with water and an extraction with dichloromethane (DCM). Unfortunately, this purification method did not work for the benzimidazole-based compound  $[\text{Ni}(\text{L2})]\text{Cl}$ . Therefore, by addition of  $\text{NH}_4\text{PF}_6$  the chloride anion was replaced with the hexafluoridophosphate counterion. The crystalline yellow needle-shaped crystals of  $[\text{Ni}(\text{L2})]\text{PF}_6$  were obtained directly from the filtrate after the reaction. The absence in the  $^1\text{H}$  NMR spectra of the nickel compounds of the characteristic downfield signals for the amide NH

and imidazolium NCHN protons indicates the successful creation of the deprotonated amide and carbene moieties and their coordination to the nickel(II) center. The ESI-MS spectra of the nickel(II) compounds exhibit base peaks corresponding to the  $[\text{M} - \text{Cl}]^+$  and  $[\text{M} - \text{PF}_6]^+$  cationic complexes (Fig. S1). Recrystallized samples of the nickel compounds were dried in vacuo before elemental analyses were performed; however, the analysis result still showed the presence of small amounts of  $\text{H}_2\text{O}$ . Compound  $[\text{Ni}(\text{L1})]\text{Cl}$  readily dissolves in water, whereas compound  $[\text{Ni}(\text{L2})]\text{PF}_6$  is soluble in DMF but hardly dissolves in water.

The cobalt-NHC compounds  $[\text{Co}(\text{L1})_2]\text{Cl}$  and  $[\text{Co}(\text{L3})_2]\text{Cl}$  were prepared using a similar method, by reacting the corresponding ligand precursors with anhydrous cobalt(II) acetate in acetonitrile or DMF in the presence of  $\text{K}_2\text{CO}_3$ . The workup procedure was performed in air, and the compounds were obtained as brown solids in a yield of 30 % and 25 %, respectively (Scheme 2). Attempts were undertaken to synthesize complexes with a 1:1 metal-to-ligand ratio by varying the ratios of the starting materials. However, only the  $[\text{Co}(\text{L2})]^+$  type complexes were obtained, which were characterized with single-crystal X-ray diffraction, NMR spectroscopy and mass spectrometry. Although a cobalt(II) salt was used in the complex synthesis, the formation of cobalt(III) complexes was apparent by the diamagnetic  $^1\text{H}$  NMR spectra of the obtained compounds (Fig. S2). The ESI-MS spectra of both cobalt complexes exhibit base peaks corresponding to the  $[\text{M} - \text{Cl}]^+$  cations (Fig. S3).



Scheme 2. Synthetic route of the complexes  $[\text{Ni}(\text{L1})]\text{Cl}$ ,  $[\text{Ni}(\text{L2})]\text{PF}_6$ ,  $[\text{Co}(\text{L1})_2]\text{Cl}$  and  $[\text{Co}(\text{L3})_2]\text{Cl}$ .

### Structural Characterization of [Ni(L1)]Cl and [Ni(L2)]PF<sub>6</sub>

Single crystals of [Ni(L1)]Cl suitable for X-ray structure determination were obtained by vapor diffusion of diethyl ether into an acetonitrile solution of the complex. Single crystals of [Ni(L2)]PF<sub>6</sub> were picked from the yellow needle-like crystals that were obtained directly from the reaction mixture. Projections of the cationic complexes are shown in Figure 1. The crystallographic and refinement data are provided in Table S1; selected bond lengths and angles are given in Table 1. The imidazole-based compound [Ni(L1)]Cl crystallized in the space group *P*<sub>2</sub><sub>1</sub>/*c*. Apart from the cationic complex and the non-coordinating chloride anion the asymmetric unit contains three lattice water molecules, which are involved in extensive intermolecular hydrogen bonds with the chloride ion and amide oxygen atom (Table S2). The benzimidazole-based compound [Ni(L2)]PF<sub>6</sub>

crystallized in the triclinic space group *P* $\bar{1}$  with one cationic complex and one PF<sub>6</sub><sup>-</sup> anion in the asymmetric unit.

In both structures the nickel(II) ion is in a four-coordinate [NiCN<sub>3</sub>] chromophore with short Ni–C (carbene) and Ni–N (amide) bonds, and two longer Ni–N (pyridine) bond lengths. Both nickel cations are found in slightly distorted square-planar geometries ( $\tau_4 = 0.18$ ) for [Ni(L1)]Cl and  $\tau_4 = 0.19$  for [Ni(L2)]PF<sub>6</sub>.<sup>[19]</sup> The Ni–N<sub>amide</sub> bonds in both complexes [1.873(3) Å and 1.8556(16) Å, respectively] are slightly longer than in other reported nickel compounds with pyridylmethyl-amide groups (ranging from 1.81 to 1.85 Å).<sup>[20–22]</sup> The carbonyl C33–O32 bond in [Ni(L1)]Cl is slightly longer than the one in [Ni(L2)]PF<sub>6</sub>, probably due to the presence of hydrogen bonds between the carbonyl O32 and lattice water molecules in [Ni(L1)]Cl (Table S2). The structure [Ni(L1)]Cl is further stabilized by intermolecular  $\pi$ – $\pi$  stacking interactions between pyridine and carbene rings with a distance of 3.52 Å. The chloride ion is at a distance of 3.44 Å of the nickel center. Intermolecular  $\pi$ – $\pi$  stacking interactions in the structure of [Ni(L2)]PF<sub>6</sub> occur between adjacent benzimidazole rings with distances of 3.53 and 3.68 Å (Figure 2).

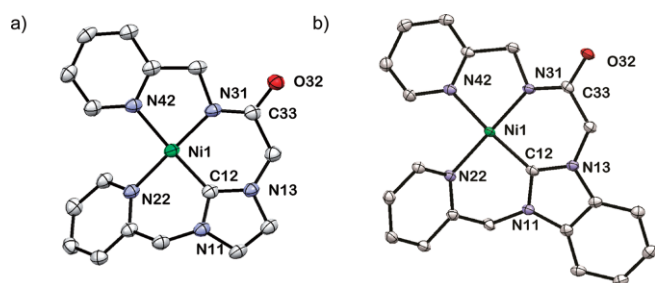


Figure 1. Displacement ellipsoid plots (50 % probability level) of the complex cations in the structures of the compounds [Ni(L1)]Cl (a) and [Ni(L2)]PF<sub>6</sub> (b) at 110(2) K. Hydrogen atoms, counterions and the lattice water solvent molecules are omitted for clarity.

### Structural Characterization of [Co(L1)<sub>2</sub>]Cl and [Co(L3)<sub>2</sub>]Cl

It appeared to be difficult to grow single crystals of [Co(L1)<sub>2</sub>]Cl suitable for X-ray structure determination. Needle-shaped single crystals were initially obtained from DCM; however, the counterion appeared to be very disordered, which made the structure refinement unsatisfactory. Block-shaped crystals were later obtained from a mixture of MeCN/H<sub>2</sub>O. The crystal that was mounted on the diffractometer was not single but rather

Table 1. Selected bond lengths [Å] and angles [°] in the structures of [Ni(L1)]Cl and [Ni(L2)]PF<sub>6</sub>.

Bond lengths [Å]	[Ni(L1)]Cl	[Ni(L2)]PF <sub>6</sub>	Angles [°]	[Ni(L1)]Cl	[Ni(L2)]PF <sub>6</sub>
Ni1–C12	1.832(3)	1.8353(19)	C12–Ni1–N31	90.76(12)	89.96(8)
Ni1–N31	1.873(3)	1.8556(16)	C12–Ni1–N22	89.36(11)	89.87(7)
Ni1–N42	1.936(2)	1.9400(16)	C12–Ni1–N42	164.85(11)	162.96(7)
Ni1–N22	1.918(2)	1.9177(16)	N31–Ni1–N22	169.26(11)	170.83(7)
C12–N13	1.336(4)	1.343(2)	N31–Ni1–N42	85.75(11)	85.62(7)
C12–N11	1.351(4)	1.349(2)	N22–Ni1–N42	96.79(10)	97.08(7)
C33–N31	1.313(4)	1.339(3)			
C33–O32	1.259(4)	1.247(2)			

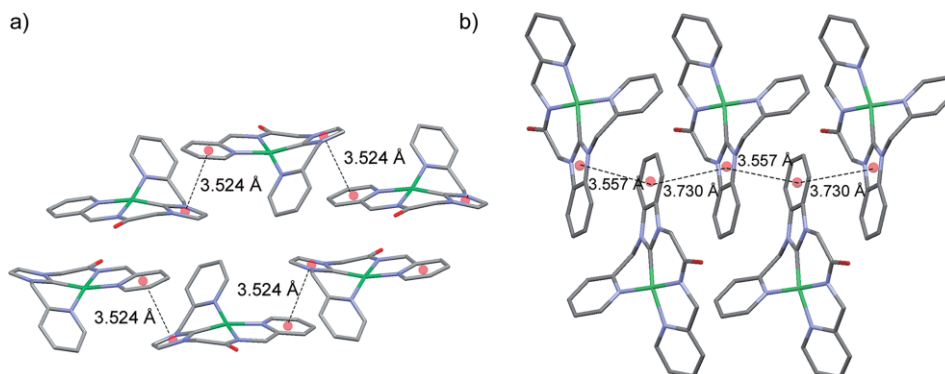


Figure 2. View of  $\pi$ – $\pi$  stacking interactions in [Ni(L1)]Cl (a) and [Ni(L2)]PF<sub>6</sub> (b). Hydrogen atoms, counterions and the lattice water solvent molecules are omitted for clarity.

a composite of two crystals related by a rotation of *ca.* 1.9° around the **b**\* direction. However, the diffraction was of good quality, and the structure refinement was problem free. The crystallographic and refinement data are provided in Table S1. For complex [Co(**L3**)<sub>2</sub>]Cl, it was difficult to grow high quality single crystals. Anion exchange was performed by adding a solution of [Co(**L3**)<sub>2</sub>]Cl in acetonitrile to a boiling acetonitrile solution of NH<sub>4</sub>PF<sub>6</sub>. Orange-colored, block-shaped crystals were obtained within one week; unfortunately, again some PF<sub>6</sub><sup>-</sup> anions as well as co-crystallized solvent molecules appeared to be severely disordered. It is assumed that the flexible benzyl arm in [Co(**L3**)<sub>2</sub>]Cl may hamper good ordering in the crystal. Similar problems concerning disorder of counterions have been reported for the structures of a number of other Co<sup>III</sup>-NHC complexes.<sup>[13,23]</sup> Despite the disorder, the general structure of the cationic complex in [Co(**L3**)<sub>2</sub>]Cl could be reliably determined from the Fourier map. Projections of the cations in [Co(**L1**)<sub>2</sub>]<sup>+</sup> and [Co(**L3**)<sub>2</sub>]<sup>+</sup> are shown in Figure 3 and Fig. S4, respectively. Selected bond lengths and angles are provided in Table S3.

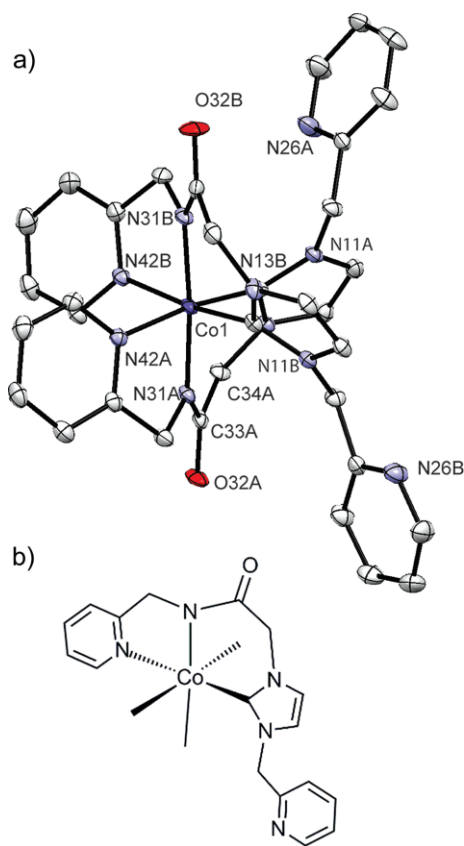


Figure 3. (a) Displacement ellipsoid plot (50 % probability level) of the cationic complex in [Co(**L1**)<sub>2</sub>]Cl at 110(2)K. The disorder, the hydrogen atoms, chloride anion and the lattice water solvent molecules are omitted for clarity. (b) Schematic drawing of the meridional, tridentate binding of **L1**<sup>-</sup> in the structure; the second ligand in the projection is bound with the pyridine nitrogen in front, the carbene carbon atom in the back.

The compound [Co(**L1**)<sub>2</sub>]Cl crystallized in the monoclinic space group *P2*<sub>1</sub>/*n*, with one complex cation, a chloride ion and two-and-a-half water molecules in the asymmetric unit. The cobalt(III) center in [Co(**L1**)<sub>2</sub>]Cl is in an octahedral coordination sphere, with two ligands bound in a tridentate, meridional fash-

ion, and thus with two uncoordinated methylpyridine groups. The meridional binding of the ligands is largely dictated by the sp<sup>2</sup> hybridization of the amide nitrogen atom. The cobalt(III) center in [Co(**L3**)<sub>2</sub>]PF<sub>6</sub> is in a similar octahedral geometry with two meridionally binding tridentate ligands, but with pendant benzyl groups. The Co–C (1.92 Å) and Co–N (1.92–1.99 Å) bonds are slightly longer than the corresponding distances in the nickel compounds. The Co–C bond lengths are similar to those in reported Co-carbene complexes.<sup>[23–28]</sup> Hydrogen bond interactions are present between the water molecules, the chloride anions and the carbonyl oxygen atoms in [Co(**L1**)<sub>2</sub>]Cl. Stacking interactions between the aromatic rings are not present in the cobalt structures.

### Electrochemical Properties of the Complexes

The redox properties of the nickel and cobalt compounds were investigated with cyclic voltammetry in dry DMF solutions containing 0.1 M tetrabutylammonium hexafluoridophosphate (TBAPF<sub>6</sub>) as the supporting electrolyte, under a stream of argon. For the imidazole-based complex [Ni(**L1**)]Cl an irreversible reduction was found at –1.4 V vs. Ag/AgCl, with the corresponding re-oxidation occurring only to a slight extent; in the anodic return scan one additional irreversible oxidative peak was found at –0.84 V (Fig. S5). The benzimidazole-based complex [Ni(**L2**)]PF<sub>6</sub> showed the first irreversible reduction at –1.27 V vs. Ag/AgCl (Figure 4). The less negative reductive potential of [Ni(**L2**)]PF<sub>6</sub> may be explained by the benzimidazole-based carbene being a more electron-withdrawing group, which makes the nickel center relatively electron poor. The oxidative peak **c** in the return scan of [Ni(**L2**)]PF<sub>6</sub> is also located at a less negative potential at –0.75 V. Upon expanding the scan window down to –2.2 V, a second irreversible reductive peak is found at –2.02 V and three small oxidative waves **c**, **d** and **e** appeared at –0.75, –0.64 and –0.26 V (Figure 4). This result indicates that the new oxidative processes **d** and **e** are related to the second

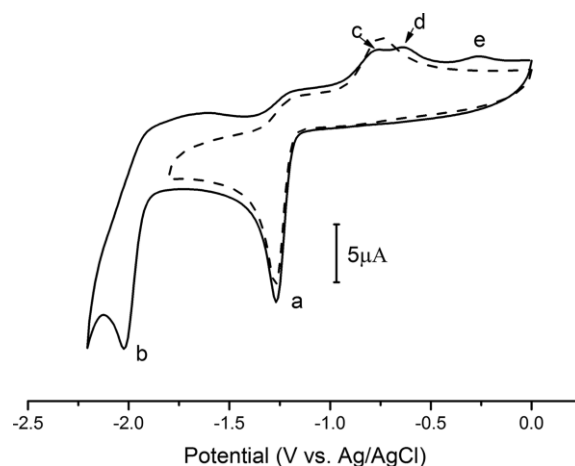


Figure 4. Cyclic voltammograms of [Ni(**L2**)]PF<sub>6</sub> (1 mM) recorded in DMF containing 0.1 M TBAPF<sub>6</sub> as supporting electrolyte in different scan windows (dashed line = 0 to –1.8 V; solid line = 0 to –2.2 V) at scan rate 0.1 V/s, using a glassy carbon working electrode. Under the used conditions the redox couple of ferrocene was located at *E*<sub>1/2</sub> = 0.52 V vs. Ag/AgCl with Δ*E* = 90–110 mV.

reductive event **b**. Thus, both  $[\text{Ni}(\text{L1})]\text{Cl}$  and  $[\text{Ni}(\text{L2})]\text{PF}_6$  show irreversible redox nature, indicating that electron transfer is immediately followed by a rapid chemical reaction or structural rearrangement.<sup>[29]</sup>

Two reversible redox couples were found for  $[\text{Co}(\text{L1})_2]\text{Cl}$  with  $E_{1/2}$  at  $-1.20$  V and  $-1.85$  V vs. Ag/AgCl (Figure 5, Table 2). In addition, two small irreversible reductive waves were found at  $-1.66$  V and  $-2.00$  V. For  $[\text{Co}(\text{L3})_2]\text{Cl}$ , the compound with two pendant benzyl groups, the two reversible redox couples appeared at  $-1.19$  V and  $-1.84$  V vs. Ag/AgCl. As the CVs of the ligand precursors do not show redox activity at these potentials (see Fig. S6), it is assumed that the two (quasi-) reversible events are metal centered. Thus, these two redox processes are tentatively assigned to the  $\text{Co}^{\text{III}}/\text{Co}^{\text{II}}$ , and  $\text{Co}^{\text{II}}/\text{Co}^{\text{I}}$  redox couples. The strong ligand-field splitting caused by the carbene and amide donor atoms clearly stabilizes the low-spin cobalt(III) centers in an octahedral geometry, resulting in very cathodic reduction potentials. Depending on the coordinating ligands and coordination geometry, the  $\text{Co}^{\text{III}}/\text{Co}^{\text{II}}$  and  $\text{Co}^{\text{II}}/\text{Co}^{\text{I}}$  redox potentials can be largely different, ranging from  $1.40$  to  $-0.83$  V vs. Ag/AgCl for  $\text{Co}^{\text{III}}/\text{Co}^{\text{II}}$  and  $-0.23$  to  $-1.38$  V vs. Ag/AgCl for  $\text{Co}^{\text{II}}/\text{Co}^{\text{I}}$ .<sup>[13,17,24]</sup> The redox potentials of the cobalt(III) compounds reported here appear to be more negative by nearly  $0.5$  V compared to reported compounds,<sup>[13,17,24]</sup> most likely because of the highly electron-donating nature of the carbene ligands. Compared to the nickel complexes, showing irreversible redox processes, the cobalt complexes are much more behaved.

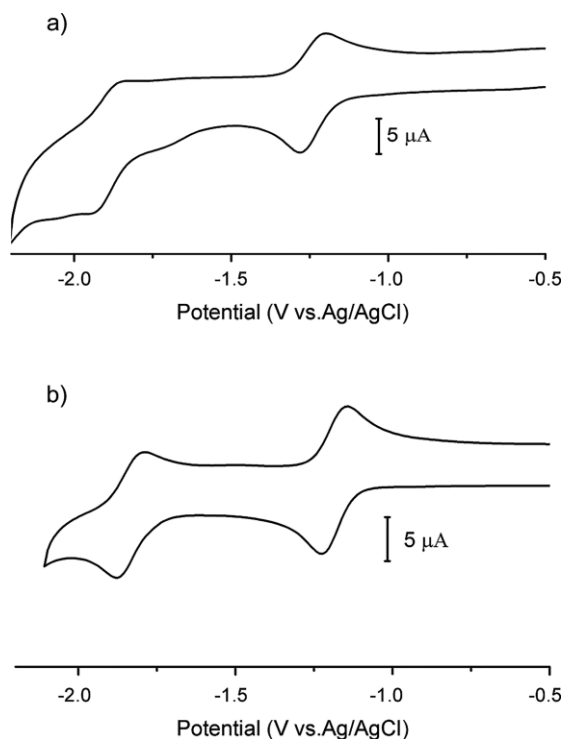


Figure 5. Cyclic voltammograms of 1 mM complex (a)  $[\text{Co}(\text{L1})_2]\text{Cl}$  and (b)  $[\text{Co}(\text{L3})_2]\text{Cl}$  in DMF containing 0.1 M TBAPF<sub>6</sub> as electrolyte at scan rate 0.1 V/s, using glassy carbon working electrode. Under the used conditions the redox couple of ferrocene was located at  $E_{1/2} = 0.52$  V vs. Ag/AgCl with  $\Delta E = 90\text{--}110$  mV. Full voltammograms of the cobalt compounds are shown in Figure 8 (dashed lines).

Table 2. Electrochemical data of the cobalt compounds.<sup>[a]</sup>

	$E_{\text{pc1}}$ [V]	$E_{\text{pa1}}$ [V]	$E_{1/2}$ [V]	$E_{\text{pc2}}$ [V]	$E_{\text{pa2}}$ [V]	$E_{1/2}$ [V]
	$E_{\text{pc1}}$ [V]	$E_{\text{pa1}}$ [V]	$(\Delta E_p)$ [mV]	$E_{\text{pc2}}$ [V]	$E_{\text{pa2}}$ [V]	$(\Delta E_p)$ [mV]
$[\text{Co}(\text{L1})_2]\text{Cl}$	-1.24	-1.16	-1.20 (80)	-1.89	-1.81	-1.85 (80)
$[\text{Co}(\text{L3})_2]\text{Cl}$	-1.23	-1.14	-1.19 (90)	-1.88	-1.79	-1.84 (90)

[a] All voltammograms were recorded in DMF; the potentials are referenced to the Ag/AgCl couple. Conditions: scan rate = 0.1 V/s, compound (1 mM), TBAPF<sub>6</sub> (0.1 M), glassy carbon working electrode. Under the used conditions the redox couple of ferrocene was located at  $E_{1/2} = 0.52$  V vs. Ag/AgCl with  $\Delta E = 90\text{--}110$  mV.

## Electrocatalytic Activity in Proton Reduction

### Compounds $[\text{Ni}(\text{L1})]\text{Cl}$ and $[\text{Ni}(\text{L2})]\text{PF}_6$

The electrocatalytic activity of the two nickel compounds for HER were studied in DMF solutions, using acetic acid as proton source. A catalytic reductive current response appeared with an onset potential at  $-1.53$  V for  $[\text{Ni}(\text{L1})]\text{Cl}$  in presence of 10 mM acid, after the reductive wave at  $-1.4$  V (Figure 6a). A similar catalytic reductive current was observed for  $[\text{Ni}(\text{L2})]\text{PF}_6$  with an

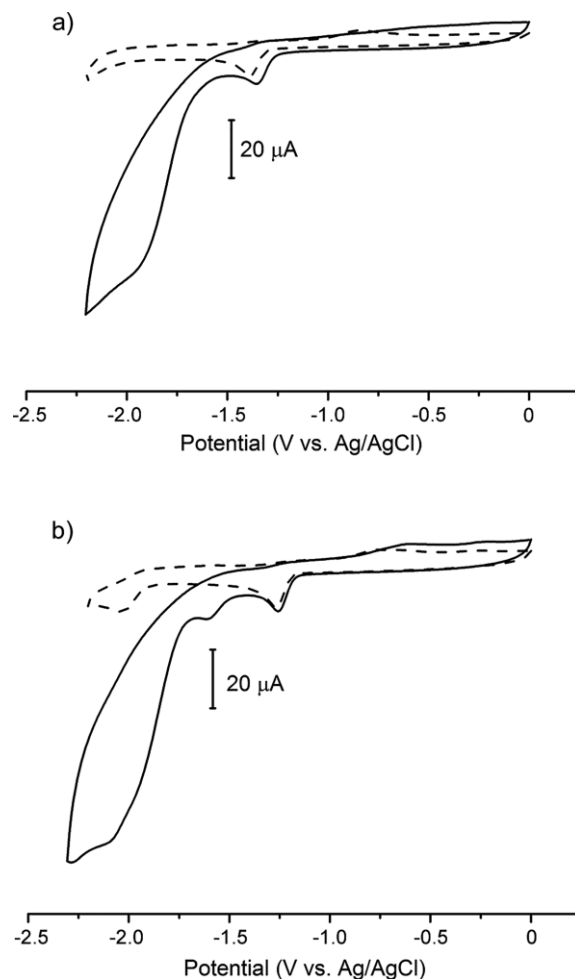


Figure 6. Cyclic voltammograms of (a) 1 mM of  $[\text{Ni}(\text{L1})]\text{Cl}$  and (b) 1 mM of  $[\text{Ni}(\text{L2})]\text{PF}_6$  recorded in DMF containing 0.1 M TBAPF<sub>6</sub> as supporting electrolyte at scan rate 0.1 V/s in absence (dashed line) and in presence (solid line) of 10 mM acetic acid, using a glassy carbon working electrode. Under the used conditions the redox couple of ferrocene was located at  $E_{1/2} = 0.52$  V vs. Ag/AgCl with  $\Delta E = 90\text{--}110$  mV.

onset potential of  $-1.69$  V. However, for  $[\text{Ni}(\text{L}2)]\text{PF}_6$  one small additional irreversible reduction appeared at  $-1.60$  V (Figure 6b). This additional peak becomes invisible with increasing acid concentration, as it is obscured by the growing catalytic peak (Fig. S7).

When the reaction concerns the two-electron transfer hydrogen evolution reaction (HER), the order of the reaction in acid can be identified using the Equation (1) and (2),<sup>[30–32]</sup> where  $x$  is the order of the reaction in protons and  $n$  is the number of electrons involved in HER ( $n = 2$ ).

$$k_{obs} = k[\text{H}^+]^x \quad (1)$$

$$\frac{i_c}{i_p} = \frac{n}{0.4463} \sqrt{\frac{RTk[\text{H}^+]^x}{Fv}} \quad (2)$$

According to Equations (1) and (2), if a plot of  $i_c/i_p$  shows a linear correlation with the square root of the proton concentration, the catalytic reaction has a first-order dependence on proton concentration. Many reports use this method to calculate  $k_{obs}$  and  $k$  for electrocatalytic reactions.<sup>[8,31,33–36]</sup>

For the complexes  $[\text{Ni}(\text{L}1)]\text{Cl}$  and  $[\text{Ni}(\text{L}2)]\text{PF}_6$ , plots of  $i_c/i_p$  vs. the square root of the acid concentration show a non-linear relationship (Fig. S8). Instead, plots of  $i_c/i_p$  vs. acid concentration do show a linear relationship (see Figure 7). This relationship reveals that two protons are involved in the rate-determining step of the reaction. Unfortunately, due to the irreversible redox properties of both compounds, Equation (2) is not suitable for

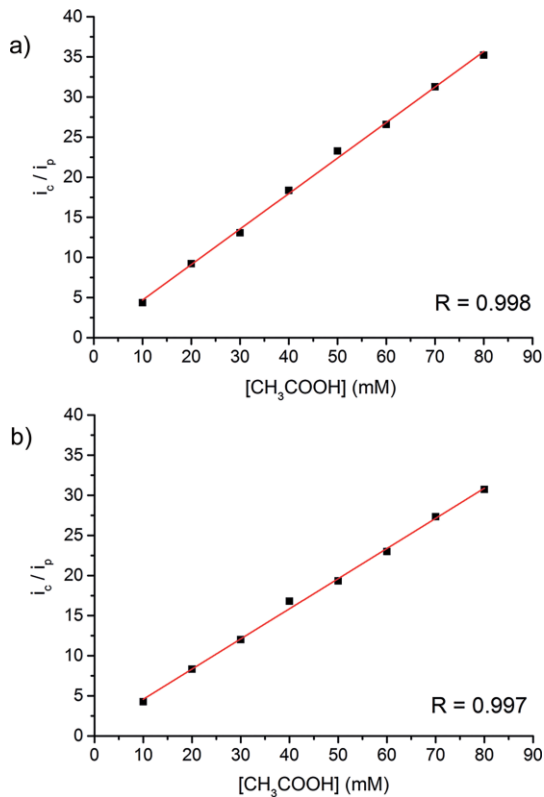


Figure 7. Plot of  $i_c/i_p$  vs.  $[\text{CH}_3\text{COOH}]$  (mM) for 1 mM  $[\text{Ni}(\text{L}1)]\text{Cl}$  (a) and 1 mM  $[\text{Ni}(\text{L}2)]\text{PF}_6$  (b) in presence of various acid concentration in DMF containing 0.1 M TBAPF<sub>6</sub> as supporting electrode at 0.1 V/s, using a glassy carbon working electrode.

determination of  $k_{obs}$ .<sup>[30,32]</sup> In the presence of 80 mM acetic acid the value of  $i_c/i_p$  reaches 35.2 and 30.7 for complex  $[\text{Ni}(\text{L}1)]\text{Cl}$  and  $[\text{Ni}(\text{L}2)]\text{PF}_6$ , respectively, indicating that the imidazole-based compound  $[\text{Ni}(\text{L}1)]\text{Cl}$  is the faster catalyst of the two for HER. This difference in activity was confirmed with controlled-potential electrolysis (CPE) experiments, as is described below.

The overpotential for proton reduction in our conditions is 860 mV for  $[\text{Ni}(\text{L}1)]\text{Cl}$  and 940 mV for  $[\text{Ni}(\text{L}2)]\text{PF}_6$ , taking homoconjugation of the acid into account.<sup>[37]</sup> In general, a more electron-donating group such as imidazolylidene will make the metal center of complex more difficult to reduce, which might increase the overpotential in electrocatalysis. The cyclic voltammograms indeed show the reductive events of  $[\text{Ni}(\text{L}1)]\text{Cl}$  to occur at more negative potentials compared to those of  $[\text{Ni}(\text{L}2)]\text{PF}_6$ . Surprisingly, the overpotential for proton reduction is lower for the imidazole-based compound.

Hydrogen production was confirmed using gas chromatography (GC; for experimental setup and data treatment see supporting information), monitoring the controlled-potential electrolysis at  $-1.8$  V; the faradaic efficiencies were determined to be around 85 % for both  $[\text{Ni}(\text{L}1)]\text{Cl}$  and  $[\text{Ni}(\text{L}2)]\text{PF}_6$ . By subtracting the results of a blank reaction (volume of H<sub>2</sub> produced at this potential in absence of catalyst), it was determined that 185  $\mu\text{L}$  and 105  $\mu\text{L}$  H<sub>2</sub> was generated over 2 h electrolysis in presence  $[\text{Ni}(\text{L}1)]\text{Cl}$  and  $[\text{Ni}(\text{L}2)]\text{PF}_6$ , respectively, corresponding to a mere 1.5 and 0.9 mol H<sub>2</sub> per mol of catalyst. The slightly better electrocatalytic activity of  $[\text{Ni}(\text{L}1)]\text{Cl}$  may tentatively be ascribed to the more electron-donating properties of the imidazole-based carbene, which might facilitate formation of a metal hydride intermediate.

Thus, the imidazole-based compound  $[\text{Ni}(\text{L}1)]\text{Cl}$  not only shows higher activity in proton reduction catalysis, but is also active at a lower overpotential, compared to the benzimidazole-based compound  $[\text{Ni}(\text{L}2)]\text{PF}_6$ . This *anti*-correlation indicates that a proton delivery between the ligand and the metal center is operative, which breaks the correlation between energy costs and kinetic barriers.<sup>[38]</sup>

#### Compound $[\text{Ni}(\text{L}1)]\text{Cl}$ in Aqueous Solution

As the compound  $[\text{Ni}(\text{L}1)]\text{Cl}$  shows good solubility in water, the electrochemical properties of  $[\text{Ni}(\text{L}1)]\text{Cl}$  were also investigated in water. Voltammograms of  $[\text{Ni}(\text{L}1)]\text{Cl}$  in an 0.2 M phosphate buffer solution (pH = 6.86) are shown in Fig. S9a. Compared to the buffer solution without nickel complex, a small irreversible reductive process at  $-1.36$  V is observed, which is followed by a large catalytic current at  $-1.82$  V, which can be assigned to the HER process. The catalytic current increases with increasing scan rate (0.05 to 2 V/s), as shown in Fig S9b. At lower scan rates the catalytic current increases linearly; at scan rates higher than 0.5 V/s, the current shows saturation (Fig. S9c).

During the electrochemical experiments, the bright yellow aqueous solution containing  $[\text{Ni}(\text{L}1)]\text{Cl}$  gradually faded to pale yellow. In order to investigate whether this color change is related to electrolysis or the stability of the compound in mildly acidic aqueous solutions, <sup>1</sup>H NMR spectra were recorded of  $[\text{Ni}(\text{L}1)]\text{Cl}$  in presence and absence of acid in D<sub>2</sub>O. The <sup>1</sup>H NMR spectra of a solution of  $[\text{Ni}(\text{L}1)]\text{Cl}$  in D<sub>2</sub>O did not change signifi-

cantly over a period of more than four days. However, upon addition of an excess of  $[D_4]$ acetic acid the color of the solution visibly faded within 1 hour, and the solution was colorless after one day. The  $^1\text{H-NMR}$  spectra revealed that nearly 50 % of the compound decomposed within 1 h (Fig. S10). The composition of the colorless solution was investigated with ESI-MS (Fig. S11). The MS peaks located at  $m/z$  309.3 and 310.3 can be assigned to the ligand precursor  $[\text{HDL1}]^+$  and  $[\text{D}_2\text{L1}]^+$ . Although the nickel compounds appear to be fairly stable in organic solvent in presence of acid (Fig. S12), it appears that the presence of even a weak acid in aqueous solution is sufficient to cause dissociation of the ligand from the nickel center by protonation of the amidate nitrogen and the carbene carbon atoms.

### Compounds $[\text{Co}(\text{L1})_2]\text{Cl}$ and $[\text{Co}(\text{L3})_2]\text{Cl}$

For both cobalt compounds the electrocatalytic activity in proton reduction was determined in DMF, using acetic acid as the proton source. In the presence of low acid concentrations (10 eq acid) using  $[\text{Co}(\text{L1})_2]\text{Cl}$  as the catalyst, two irreversible reductive peaks were found at  $-1.16$  and  $-1.45$  V, followed by an obvious catalytic wave at  $-1.78$  V vs. Ag/AgCl. Compound  $[\text{Co}(\text{L3})_2]\text{Cl}$  gave a similar result, the CV showing two irreversible reduction peaks at  $-1.17$  and  $-1.32$  V, followed by a catalytic wave at  $-1.81$  V (Figure 8). The first reductive event occurs at slightly more positive potentials than the  $\text{Co}^{\text{III}}/\text{Co}^{\text{II}}$  reductive event in the absence of acid. A new reduction process seems to be present at a potential that is much more positive than the reductive wave tentatively ascribed to the  $\text{Co}^{\text{II}}/\text{Co}^{\text{I}}$  couple, that in the absence of acid is located around  $-1.8$  V (Figure 5).

The CV of a solution of the acid in DMF in the absence of catalyst, the CV of the ligand precursor  $\text{H}_2\text{L1Cl}$  in the presence of acid, and the CV of the complex  $[\text{Co}(\text{L1})_2]\text{Cl}$  are compared in Fig. S13. The CV of pure acid does not show a significant catalytic current and the CV of the ligand precursor  $\text{H}_2\text{L1Cl}$  shows a small reductive wave. Thus the catalytic current found in the presence of the coordination compound is related to the cobalt redox couple.

The voltammograms obtained for complex  $[\text{Co}(\text{L1})_2]\text{Cl}$  in varying concentrations of acid are shown in Figure 9. The catalytic current increases with increasing concentrations of the acid, and the onset potential of the catalytic peak gradually shifts to more positive potentials. This shift in onset potential indicates that a proton-coupled electron-transfer (PCET) process is operative.<sup>[39,40]</sup>

A large catalytic current  $\{i_c/i_p = 62$  for  $[\text{Co}(\text{L1})_2]\text{Cl}$  and  $i_c/i_p = 28$  for  $[\text{Co}(\text{L3})_2]\text{Cl}\}$  is observed at 70 eq acid concentration at a scan rate of 0.1 V/s, with an overpotential of 830 mV for  $[\text{Co}(\text{L1})_2]\text{Cl}$  and 940 mV for  $[\text{Co}(\text{L3})_2]\text{Cl}$ . The complex  $[\text{Co}(\text{L1})_2]\text{Cl}$  shows a smaller overpotential, largely due to the PCET process. For both  $[\text{Co}(\text{L1})_2]\text{Cl}$  and  $[\text{Co}(\text{L3})_2]\text{Cl}$  plots of  $i_c/i_p$  show a linear relationship with the square root of acid concentration (Figure 10), indicating the reaction to be first-order with respect to acid concentration.

Similarly, the production of hydrogen gas was confirmed and quantified using GC, monitoring CPE at  $-1.8$  V. The faradaic efficiencies were determined to be 77 % for  $[\text{Co}(\text{L3})_2]\text{Cl}$  and 82 % for  $[\text{Co}(\text{L1})_2]\text{Cl}$ . By subtracting the blank it was calculated that

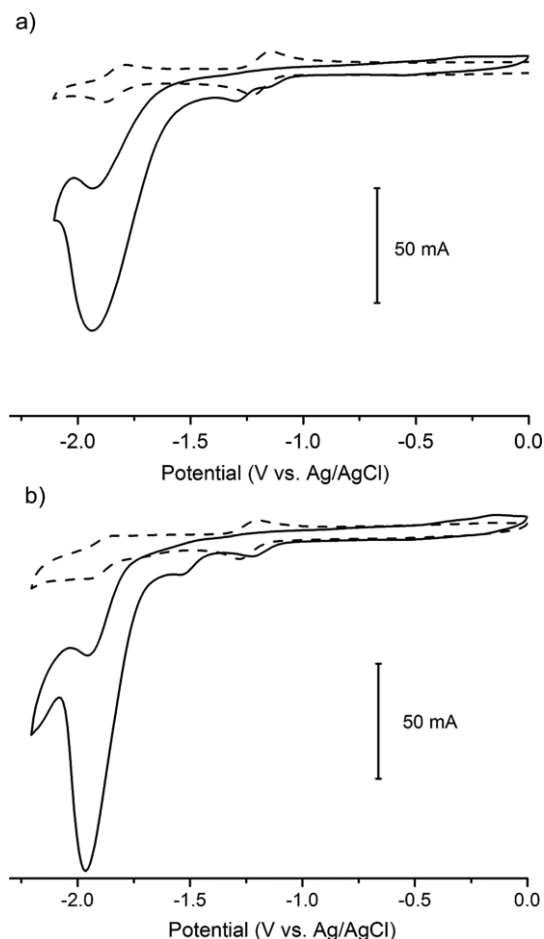


Figure 8. Cyclic voltammograms of 1 mM complex  $[\text{Co}(\text{L1})_2]\text{Cl}$  (a) and  $[\text{Co}(\text{L3})_2]\text{Cl}$  (b) in absence (dashed line) and in presence (solid line) of 10 mM acetic acid in DMF containing 0.1 M  $\text{TBAPF}_6$  as electrolyte at scan rate 0.1 V/s, using glassy carbon working electrode. Under the used conditions the redox couple of ferrocene was located at  $E_{1/2} = 0.52$  V vs. Ag/AgCl with  $\Delta E = 90\text{--}110$  mV.

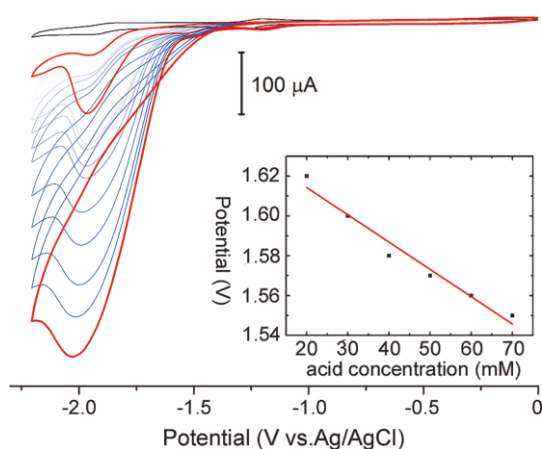


Figure 9. Cyclic voltammograms of  $[\text{Co}(\text{L1})_2]\text{Cl}$  (1 mM) in presence of various concentrations of acetic acid (0–70 mM), in DMF. Inset: plot of the onset potential as a function of acid concentration ( $R^2 = 0.96$ ). Conditions: Scan rate 0.1 V/s,  $\text{TBAPF}_6$  (0.1 M), glassy-carbon working electrode. Under the used conditions the redox couple of ferrocene was located at  $E_{1/2} = 0.52$  V vs. Ag/AgCl with  $\Delta E = 90\text{--}110$  mV.

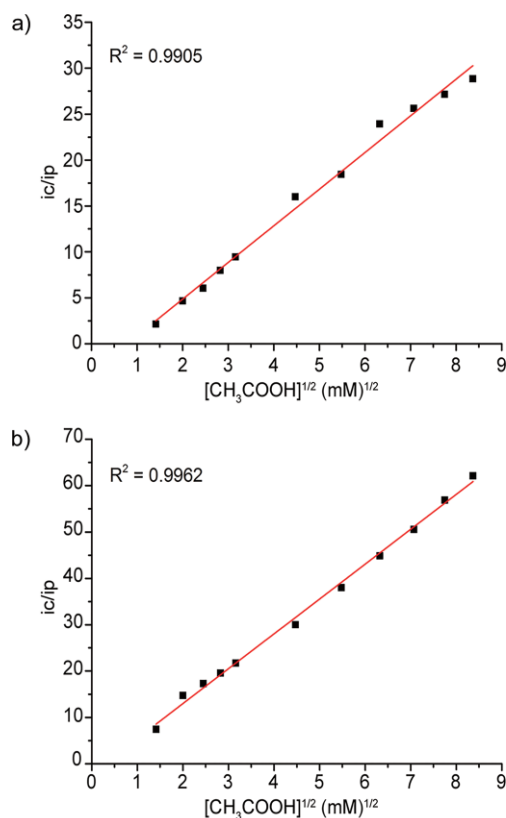


Figure 10. Plots of  $i_c/i_p$  vs.  $[CH_3COOH]^{1/2}$  (mM)<sup>1/2</sup> for 1 mM [Co(L1)<sub>2</sub>]Cl (a) and 1 mM [Co(L3)<sub>2</sub>]Cl (b) in DMF. Conditions: TBAPF<sub>6</sub> (0.1 M), scan rate 0.1 V/s, glassy carbon working electrode.

75  $\mu$ L and 145  $\mu$ L H<sub>2</sub> was generated in presence of 1 mM [Co(L3)<sub>2</sub>]Cl and [Co(L1)<sub>2</sub>]Cl, respectively, over 2 h electrolysis, corresponding to 0.6 and 1.2 mol H<sub>2</sub> per mol of catalyst.

In order to investigate how the complexes might interact with protons in electrocatalysis, excess [D<sub>4</sub>]acetic acid was added to the complex [Co(L1)<sub>2</sub>]Cl or [Co(L3)<sub>2</sub>]Cl in [D<sub>3</sub>]acetonitrile (Fig. S14 and Fig. S15). For complex [Co(L1)<sub>2</sub>]Cl, with two pendant pyridine groups, the resonances of alkyl protons shift down field in presence of acid (Fig. S14). This is ascribed to protonation of the free pyridine groups as well as the amide oxygen, as the NMR spectra of [Co(L3)<sub>2</sub>]Cl also showed the resonances of the alkyl protons to shift downfield in presence of acid, notably the protons adjacent to the amide (Fig. S15). The protonation is confirmed by the ESI-MS spectrum of the NMR sample (Fig. S16): peaks are found centered at  $m/z = 674.7$  and 337.5, which can be attributed to [Co(L1)<sub>2</sub>]<sup>+</sup> and [Co(L1)<sub>2</sub> + D]<sup>2+</sup> fragments in which varying numbers of hydrogens of the ligand are substituted with deuterons. Importantly, no additional peaks appeared upon addition of an excess of acid, indicating that both complexes are stable in acidic organic solutions.

## Conclusion

Three pyridyl-amide substituted (benz)imidazolium salts H<sub>2</sub>L1Cl, H<sub>2</sub>L2Cl, and H<sub>2</sub>L3Cl were synthesized and successfully employed as ligand precursors for the syntheses of novel

nickel(II) and cobalt(III) complexes. The nickel ions in [Ni(L1)]Cl and [Ni(L2)]PF<sub>6</sub> are in slightly distorted square-planar geometries, whereas the cobalt ions in [Co(L1)<sub>2</sub>]Cl and [Co(L3)<sub>2</sub>]Cl are in octahedral geometries. Although the ligand H<sub>2</sub>L1Cl in combination with Ni<sup>II</sup> ions forms square-planar coordination compounds with the binding of only one ligand, we were unable to obtain cobalt compounds with only one ligand coordinated. The strong ligand-field splitting caused by the carbene and amide donor atoms clearly stabilizes low-spin cobalt(III) centers in an octahedral geometry. More sterically hindering groups should be employed as pendant groups to be able to generate a cobalt(II) compound in a square-planar, tetrahedral or 5-coordinate geometry.

Cyclic voltammetry of the two nickel compounds showed irreversible redox events, whereas the CVs. of the two cobalt compounds revealed two reversible redox events. In DMF in presence of acetic acid the four compounds show electrocatalytic activity in proton reduction as confirmed by CV measurements and quantified with GC. The imidazole-based complex [Ni(L1)]Cl shows slightly higher catalytic activity at lower overpotentials than the benzimidazole-based compound [Ni(L2)]PF<sub>6</sub>. The saturated coordination sphere of the cobalt(III) ion in [Co(L1)<sub>2</sub>]Cl and [Co(L3)<sub>2</sub>]Cl in principle makes it difficult to form a cobalt-hydride intermediate, which is essential in the catalytic proton reduction reaction. During turnover at least one of the ligands should dissociate from the cobalt center; most likely this will be one of the coordinating pyridyl nitrogen atoms. The NMR and MS study with the addition of acid indicates that this dissociation does not occur in the Co<sup>III</sup> species, as the aromatic region in the NMR spectra of [Co(L3)<sub>2</sub>]Cl does not change upon addition of acid. Thus, dissociation of the pyridyl nitrogen and subsequent protonation must occur after reduction of the cobalt(III) center to cobalt(II). As for cobalt(II) a five-coordinate species is quite common, dissociation of one of the ligands upon reduction of the cobalt center is a feasible event. The complex [Co(L1)<sub>2</sub>]Cl exhibits a smaller overpotential and higher catalytic activity than [Co(L3)<sub>2</sub>]Cl, largely due to the PCET process that most likely is facilitated by the presence of the pendant pyridine groups. Although the rate of electrolysis could not be established for the nickel compounds, based on the amount of dihydrogen gas formed after 2 h of electrolysis it appears that [Ni(L1)]Cl is a better electrocatalyst for HER than [Co(L1)<sub>2</sub>]Cl, despite the fact that the latter compound benefits from the presence of pendant pyridyl groups.

Combined with earlier results,<sup>[14–16]</sup> we believe that the presence of pendant pyridine groups indeed facilitates proton transfer in solution. Nevertheless, the large overpotentials and rather poor catalytic activity of the compounds described in this paper lead us to conclude that the carbene ligands are too electron-donating to be applied as auxiliary ligands for HER catalysts. Be that as it may, the reported new compounds might be still attractive for other purposes: the synthesis route of the complexes is straightforward, and the complexes are air and moisture stable. This report thus provides knowledge on the design of transition-metal molecular catalyst and gives useful information for those considering to apply carbene complexes in electrocatalysis.

## Experimental Section

**Materials:** Commercial chemicals were used without further purification. Acetonitrile, tetrahydrofuran, dichloromethane and diethyl ether were obtained from a PureSolv MD5 solvent dispenser. Dry ethanol and dimethylformamide were obtained by adding molecular sieves into the commercial anhydrous solvent. The other commercial solvents were used without further purification. All air-sensitive reactions were performed under argon or dinitrogen gas using standard Schlenk techniques unless mentioned otherwise. The compounds dichlorido(dimethoxyethane)nickel  $\{[\text{Ni}(\text{dme})\text{Cl}_2]\}$ ,<sup>[41]</sup> 2-chloro-*N*-(pyridin-2-ylmethyl)acetamide,<sup>[42]</sup> and *N*-pyridin-2-ylmethyl(benz)imidazole<sup>[43]</sup> were prepared following published procedures. The ligand precursor  $\text{H}_2\text{L3Cl}$  was synthesized following a literature method.<sup>[18]</sup>

**Analytical Methods:**  $^1\text{H}$  and  $^{13}\text{C}$  spectra were recorded on Bruker 300DPX/400DPX-liq spectrometer. Mass spectra were obtained using a Finnigan Aqueous Mass Spectrometer (MS) with electrospray ionization (ESI). Elemental analyses were performed by the Mikroanalytisches Laboratorium Kolbe, Germany. Cyclic voltammograms were recorded with an Autolab PGstat10 potentiostat controlled by GPES4 software under argon. A 3 mm diameter glassy-carbon electrode was used as working electrode and a platinum wire as the counter electrode. The experimental reference electrode was a commercially available Ag/AgCl electrode. Ferrocene was added at the end of each measurement as an internal standard when experiments were carried out in organic solvents. Under the used conditions the redox couple of ferrocene was located at  $E_{1/2} = 0.52\text{ V}$  vs. Ag/AgCl with  $\Delta E = 90\text{--}110\text{ mV}$ .

Controlled-potential electrolysis (CPE) experiments were carried out in an H-shaped double-compartment cell, connected to a gas chromatograph (see Fig. S17). A glassy-carbon electrode with a surface area of  $0.07\text{ cm}^2$  was used as the working electrode for electrolysis. As the auxiliary electrode a platinum gauze electrode was used. The reference electrode was a commercially available aqueous Ag/AgCl electrode. The solution containing the sample was bubbled with helium gas for 10 min before measurement and the electrolysis was carried out under an atmosphere of helium. The solutions in both compartments were constantly stirred during electrolysis experiments. The evolved  $\text{H}_2$  gas produced during electrolysis measurements was quantified using gas chromatography, which was performed on a Shimadzu GC2010 at  $35\text{ }^\circ\text{C}$  fitted with a Supelco Carboxen 1010 molecular sieve column. Two separate experiments were done and the results of two experiments were averaged. See supporting information for a description of the procedures and data handling.

**Single Crystal X-ray Crystallography:** For both nickel complexes, all reflection intensities were measured at  $110(2)\text{ K}$  using a SuperNova diffractometer (equipped with Atlas detector) with  $\text{Cu-K}\alpha$  radiation ( $\lambda = 1.54178\text{ \AA}$ ) under the program CrysAlisPro (Version 1.171.37.35 Agilent Technologies, 2014). The same program was used to refine the cell dimensions and for data reduction. The structure was solved with the program SHELXS-2014/7 and was refined on  $F^2$  with SHELXL-2014/7.<sup>[44]</sup> Analytical numeric absorption correction using a multifaceted crystal model was applied using CrysAlisPro. The temperature of the data collection was controlled using the system Cryojel (manufactured by Oxford Instruments). The H atoms were placed at calculated positions (unless otherwise specified) using the instructions AFIX 23 or AFIX 43 with isotropic displacement parameters having values  $1.2\text{ Ueq}$  of the attached C atoms.

For compound  $[\text{Co}(\text{L1})_2]\text{Cl}$ , all reflection intensities were measured at  $110(2)\text{ K}$  using a SuperNova diffractometer (equipped with Atlas

detector) with  $\text{Mo-K}\alpha$  radiation ( $\lambda = 0.71073\text{ \AA}$ ) under the program CrysAlisPro (Version CrysAlisPro 1.171.39.29c, Rigaku OD, 2017). The same program was used to refine the cell dimensions and for data reduction. The structure was solved with the program SHELXS-2014/7 (Sheldrick, 2015) and was refined on  $F^2$  with SHELXL-2014/7 (Sheldrick, 2015).<sup>[44]</sup> Numerical absorption correction based on gaussian integration over a multifaceted crystal model was applied using CrysAlisPro. The temperature of the data collection was controlled using the system Cryojel (manufactured by Oxford Instruments). The H atoms were placed at calculated positions (unless otherwise specified) using the instructions AFIX 23 or AFIX 43 with isotropic displacement parameters having values  $1.2\text{ Ueq}$  of the attached C atoms. The H atoms attached to O1W/O2W/O3W were found from difference Fourier maps (the locations of the H atoms attached to O2W are probably not very accurate as the H atoms might be disordered), and their coordinates were refined freely [the O–H and H...H bond lengths were restrained to be  $0.84(3)$  and  $1.33(3)\text{ \AA}$  using the DFIX instruction]. The structure is partly disordered.

CCDC 1521419 (for  $[\text{Ni}(\text{L1})\text{Cl}]$ ), 1521420 (for  $[\text{Ni}(\text{L2})\text{PF}_6]$ ), and 1578239 (for  $[\text{Co}(\text{L1})_2]\text{Cl}$ ) contain the supplementary crystallographic data for this paper. These data can be obtained free of charge from The Cambridge Crystallographic Data Centre.

### Additional Notes for the Structures

**$[\text{Ni}(\text{L1})\text{Cl}]$ :** The H atoms attached to O1W/O2W/O2W' (minor component)/O3W (but not O3W') were found from difference Fourier maps, and their coordinates were refined semi-freely using a set of DFIX restraints to keep the O–H and H...H values within acceptable ranges. The structure is mostly ordered. The asymmetric contains three lattice water solvent molecules. Two are disordered over two orientations, and the occupancy factors of the major components of the disorder refine to  $0.721(6)$  and  $0.858(6)$ . The H atoms for O3W' could not be retrieved. Apart from the hydrogen bonds between carbonyl and water molecules, there are specified hydrogen bonds between chloride ion and water molecules (hydrogen bond details are provided in the supporting information).

**$[\text{Ni}(\text{L2})\text{PF}_6]$ :** The structure is partly disordered. The  $\text{PF}_6^-$  counterion is found to be disordered over two orientations; the occupancy factor of the major component of the disorder refines to  $0.869(9)$ .

**$[\text{Co}(\text{L1})_2]\text{Cl}$ :** The fragment-N13B is disordered over two orientations. The occupancy factors of the major component of the disorder refines to  $0.519(9)$ . The lattice water molecule O3W has an occupancy factor of  $0.5$  as it is found on an inversion center. The crystal that was mounted on the diffractometer was not a single crystal, but rather a composite of two crystals related by a rotation of  $ca. 1.9^\circ$  around the reciprocal direction  $[-0.02\ 1.00\ 0.07]$ . The BASF scale factor refines for  $0.0366(18)$ .

**$[\text{Co}(\text{L3})_2]\text{PF}_6$ :** only the structure of the cationic complex could be determined. The counterions are severely disordered hampering full refinement of the structure.

### Ligand and Complex Synthesis

**$\text{H}_2\text{L1Cl}$ :** *N*-pyridin-2-ylmethylimidazole ( $6\text{ mmol}$ ,  $0.960\text{ g}$ ) and 2-chloro-*N*-(pyridin-2-ylmethyl)acetamide ( $5\text{ mmol}$ ,  $0.925\text{ g}$ ) were added into a  $100\text{ mL}$  round-bottomed flask containing  $25\text{ mL}$  of dry ethanol. The mixture was heated at  $80\text{ }^\circ\text{C}$  for  $5\text{ h}$ , after which the solvent was removed by rotary evaporation. The residue was dissolved in THF and the solution was filtered. The filtrate was con-

centrated to 5 mL and acetone was added until a yellow precipitate appeared. The yellow-brownish powder was collected by filtration, washed with diethyl ether, and dried under vacuum. Yield: 0.92 g (54 % based on the acetamide).  $^1\text{H}$  NMR (300 MHz,  $[\text{D}_6]\text{DMSO}$ )  $\delta$  = 9.32 (s, 1H, NCHN), 9.15 (t,  $J$  = 5.6 Hz, 1H, NH), 8.54 (dd,  $J$  = 11.4, 4.8 Hz, 2H, Py-H), 7.89 (td,  $J$  = 7.7, 1.8 Hz, 1H, Py-H), 7.78 (m, 3H, Py-H), 7.54–7.21 (m, 4H, Py-H,  $\text{C}_{\text{imidazole-H}}$ ), 5.62 (s, 2H, Py- $\text{CH}_2\text{-N}_{\text{imidazole}}$ ), 5.17 (s, 2H, Py- $\text{CH}_2\text{-N}_{\text{amide}}$ ), 4.44 [d,  $J$  = 5.8 Hz, 2H, C(O)- $\text{CH}_2\text{-N}_{\text{imidazole}}$ ].  $^{13}\text{C}$  NMR (75 MHz,  $[\text{D}_6]\text{DMSO}$ )  $\delta$  = 165.13, 157.60, 153.57, 149.61, 148.94, 137.54, 136.79, 123.96, 123.68, 122.59, 122.49, 122.35, 121.32, 53.05, 50.65, 44.42. The signal of N-CH-N could not be found. ESI-MS found (calc):  $[\text{M}-\text{Cl}]^+$   $m/z$  308.2 (308.15).

**H<sub>2</sub>L2Cl:** The synthetic procedure of HL1Cl was followed, but with the starting material *N*-pyridin-2-ylmethylbenzimidazole (8.5 mmol, 1.78 g) and 2-chloro-*N*-(pyridin-2-ylmethyl)acetamide (8.5 mmol, 1.6 g) in 25 mL of dry ethanol at 80 °C for 60 h. Yield: 0.90 g (30 % based on the acetamide).  $^1\text{H}$  NMR (300 MHz,  $[\text{D}_6]\text{DMSO}$ )  $\delta$  = 10.02 (s, 1H, NCHN), 9.44 (s, 1H, NH), 8.56 (d,  $J$  = 4.7 Hz, 1H, Py-H), 8.49 (d,  $J$  = 4.6 Hz, 1H, Py-H), 8.02 (d,  $J$  = 7.1 Hz, 1H, Py-H), 7.98–7.81 (m, 3H, Py-H), 7.73–7.59 (m, 3H, Py-H,  $\text{C}_{\text{benzimidazole-H}}$ ), 7.46 (d,  $J$  = 7.8 Hz, 1H,  $\text{C}_{\text{benzimidazole-H}}$ ), 7.37 (q,  $J$  = 7.7 Hz, 2H,  $\text{C}_{\text{benzimidazole-H}}$ ), 5.99 (s, 2H, Py- $\text{CH}_2\text{-N}_{\text{benzimidazole}}$ ), 5.55 (s, 2H, Py- $\text{CH}_2\text{-N}_{\text{amide}}$ ), 4.51 [s, 2H, C(O)- $\text{CH}_2\text{-N}_{\text{benzimidazole}}$ ].  $^{13}\text{C}$  NMR (75 MHz,  $[\text{D}_6]\text{DMSO}$ )  $\delta$  = 165.07, 152.99, 149.67, 148.29, 144.16, 137.63, 131.65, 130.95, 126.76, 123.79, 122.81, 122.70, 121.71, 113.91, 50.92, 48.66, 44.14. ESI-MS found (calc):  $[\text{M}-\text{Cl}]^+$   $m/z$  358.2 (358.17).

**[Ni(L1)]Cl:** A Schlenk flask was charged with  $[\text{Ni}(\text{dme})\text{Cl}_2]$  (0.5 mmol, 0.11 g),  $\text{H}_2\text{L1Cl}$  (0.5 mmol, 0.17 g),  $\text{K}_2\text{CO}_3$  (1.9 mmol, 0.26 g) and dry DMF (10 mL) under an argon atmosphere. The dark green solution was stirred at room temperature overnight, after which the reaction mixture was filtered to remove the salts. To the filtrate 100 mL of distilled water was added and the aqueous solution was washed with DCM (3 × 50 mL). The water layer was evaporated to dryness. The resulting yellow solid was collected and dried under vacuum. Crystals suitable for X-ray structure determination were obtained by vapor diffusion of diethyl ether into an acetonitrile solution of the complex. Yield: 28 % (56 mg).  $^1\text{H}$  NMR (300 MHz,  $[\text{D}_6]\text{DMSO}$ )  $\delta$  = 9.09 (d,  $J$  = 5.5 Hz, 1H, Py-H), 8.22 (t,  $J$  = 7.1 Hz, 1H, Py-H), 8.10 (t,  $J$  = 7.3 Hz, 1H, Py-H), 7.86 (d,  $J$  = 7.6 Hz, 1H, Py-H), 7.70 (m, 3H, Py-H), 7.49 (d,  $J$  = 8.6 Hz, 3H, Py-H, NCH), 5.74 (s, 2H, Py- $\text{CH}_2\text{-N}_{\text{NHC}}$ ), 4.74 (s, 2H, Py- $\text{CH}_2\text{-N}_{\text{amide}}$ ), 4.71 (broad, 2H,  $\text{C}_{\text{amide-CH}_2\text{-N}_{\text{NHC}}}$ ).  $^{13}\text{C}$  NMR (75 MHz,  $[\text{D}_6]\text{DMSO}$ )  $\delta$  = 214.87, 168.08, 163.85, 154.40, 153.52, 149.09, 147.32, 140.51, 139.53, 125.64, 123.37, 122.38, 122.08, 121.19, 58.04, 52.27, 51.92. Anal. Calcd for  $\text{C}_{17}\text{H}_{16}\text{ClN}_5\text{NiO} \cdot 1.5\text{H}_2\text{O}$ : C 47.76, H 4.48, N 16.38; found C 47.58, H 4.78, N 16.25. ESI-MS found (calc):  $[\text{M}-\text{Cl}]^+$   $m/z$  364.1 (364.07).

**[Ni(L2)]PF<sub>6</sub>:** A Schlenk flask was charged with  $[\text{Ni}(\text{dme})\text{Cl}_2]$  (0.5 mmol, 0.11 g),  $\text{H}_2\text{L2Cl}$  (0.5 mmol, 0.195 g),  $\text{NH}_4\text{PF}_6$  (0.5 mmol, 0.10 g),  $\text{K}_2\text{CO}_3$  (1.9 mmol, 0.26 g) and dry DMF (10 mL) under an argon atmosphere. The brown solution was stirred at room temperature for 2 days. The reaction mixture was filtered and the filtrate was left standing for a few days, during which time yellow crystals formed. The crystalline solid was collected by filtration, washed with diethyl ether and dried under vacuum. Yield: 22 % (60 mg). Yellow needle crystals suitable for X-ray structure determination were obtained directly from filtrate after the reaction. The compound is poorly soluble in DMSO.  $^1\text{H}$  NMR (400 MHz,  $[\text{D}_3]\text{acetonitrile}$ )  $\delta$  = 8.93 (d,  $J$  = 5.6 Hz, 2H, Py-H), 8.12 (t,  $J$  = 7.7 Hz, 1H, Py-H), 8.01 (t,  $J$  = 7.7 Hz, 1H, Py-H), 7.80 (dd,  $J$  = 16.2, 7.9 Hz, 2H, NCH), 7.62 (m, 3H, Py-H), 7.48 (m, 3H, Py-H, Ar-H), 7.34 (t,  $J$  = 6.6 Hz, 1H, Ar-H), 5.79 (s, 2H, Py- $\text{CH}_2\text{-N}_{\text{NHC}}$ ), 4.89 (s, 2H, Py- $\text{CH}_2\text{-N}_{\text{amide}}$ ), 4.82 (broad, 2H,  $\text{C}_{\text{amide-CH}_2\text{-N}_{\text{NHC}}}$ ).  $^{13}\text{C}$  NMR (101 MHz,  $[\text{D}_3]\text{acetonitrile}$ )  $\delta$  = 154.40,

148.69, 141.76, 140.89, 127.05, 126.88, 125.33, 125.26, 124.41, 122.32, 112.35, 111.93, 59.50, 50.85, 50.52. The six quaternary carbons could not be detected due to the low concentration caused by the limited solubility of the compound. Anal. Calcd for  $\text{C}_{21}\text{H}_{18}\text{F}_6\text{N}_5\text{NiO}$ : C 45.03, H 3.24, N 12.50; found C 44.26, H 3.42, N 12.07. ESI-MS found (calc):  $[\text{M}-\text{PF}_6]^+$   $m/z$  414.1 (414.09).

**[Co(L1)<sub>2</sub>]Cl:** A Schlenk flask was charged with anhydrous cobalt(II) acetate (0.85 mmol, 0.15 g),  $\text{H}_2\text{L1Cl}$  (0.85 mmol, 0.29 g),  $\text{K}_2\text{CO}_3$  (3.4 mmol, 0.47 g) and dry  $\text{CH}_3\text{CN}$  (10 mL) under an  $\text{N}_2$  atmosphere. To this mixture 2 mL of DMF was added. The dark brown suspension was stirred at room temperature for 2 days. The reaction mixture was filtered to remove the insoluble products, and the filtrate was added dropwise into 100 mL of diethyl ether. The yellow-brown solid was collected by filtration, redissolved in anhydrous acetonitrile and passed through a short Celite column. The solution was concentrated to around 2 mL and added dropwise into diethyl ether to result in a light brown solid. Yield: 30 % (90 mg). Single crystals of  $[\text{Co}(\text{L1})_2]\text{Cl}$  for X-ray structure determination were obtained from a DCM solution of complex in 3 days.  $^1\text{H}$  NMR (300 MHz,  $[\text{D}_3]\text{acetonitrile}$ )  $\delta$  = 8.42 (dd,  $J$  = 17.9, 4.8 Hz, 2H, Py-H), 7.90 (d,  $J$  = 5.7 Hz, 2H, Py-H), 7.76–7.62 (m, 4H, Py-H), 7.43 (d,  $J$  = 7.8 Hz, 2H, Py-H), 7.20 (q,  $J$  = 7.0 Hz, 4H, Py-H), 7.12 (d,  $J$  = 1.8 Hz, 2H,  $\text{C}_{\text{imidazole-H}}$ ), 7.02 (d,  $J$  = 7.8 Hz, 2H, Py-H), 6.87 (d,  $J$  = 2.0 Hz, 2H,  $\text{C}_{\text{imidazole-H}}$ ), 5.30 (d,  $J$  = 18.8 Hz, 2H, Py- $\text{CHH-N}_{\text{NHC}}$ ), 4.98 (d,  $J$  = 15.8 Hz, 2H, Py- $\text{CHH-N}_{\text{amide}}$ ), 4.79 (d,  $J$  = 15.8 Hz, 2H, Py- $\text{CHH-N}_{\text{amide}}$ ), 4.65–4.46 [m, 4H, C(O)- $\text{CHH-N}_{\text{NHC}}$ , Py- $\text{CHH-N}_{\text{imidazole}}$ ], 4.37 [d,  $J$  = 17.0 Hz, 2H, C(O)- $\text{CHH-N}_{\text{imidazole}}$ ].  $^{13}\text{C}$  NMR (75 MHz,  $[\text{D}_3]\text{acetonitrile}$ )  $\delta$  = 170.07, 164.36, 155.26, 150.38, 149.18, 139.87, 138.05, 126.39, 125.26, 124.82, 124.00, 123.26, 122.70, 55.92, 55.78, 53.28. ESI-MS found (calculated):  $[\text{M}-\text{Cl}]^+$   $m/z$  671.1 (671.2).

**[Co(L3)<sub>2</sub>]Cl:** A Schlenk flask was charged with commercially available anhydrous cobalt(II) acetate (0.35 mmol, 0.06 g),  $\text{H}_2\text{L3Cl}$  (0.7 mmol, 0.17 g),  $\text{K}_2\text{CO}_3$  (2.68 mmol, 0.37 g) and dry DMF (10 mL) under an  $\text{N}_2$  atmosphere. The dark brown solution was stirred at room temperature for 2 days. The reaction mixture was filtered to remove the insoluble products and the filtrate was added dropwise into 100 mL of diethyl ether. The formed yellow-brown solid was collected by filtration and redissolved in anhydrous acetonitrile. This solution was passed through a short celite column. The solution was concentrated to around 2 mL, and then was added dropwise into diethyl ether to result in a light brown solid. Yield: 25 % (60 mg).  $^1\text{H}$  NMR (400 MHz,  $[\text{D}_3]\text{acetonitrile}$ )  $\delta$  = 7.95 (d,  $J$  = 5.5 Hz, 2H, Py-H), 7.66 (td,  $J$  = 7.7, 1.4 Hz, 2H, Py-H), 7.38 (d,  $J$  = 7.8 Hz, 2H, Py-H), 7.29–7.24 (m, 6H, Ar-H), 7.22 (d,  $J$  = 7.22 Hz, 2H, Py-H), 7.20 (d,  $J$  = 5.5 Hz, 2H,  $\text{C}_{\text{imidazole-H}}$ ), 6.82 (d,  $J$  = 2.0 Hz, 2H,  $\text{C}_{\text{imidazole-H}}$ ), 6.78 (dd,  $J$  = 5.5, 3.7 Hz, 4H, Ar-H), 5.05 (d,  $J$  = 19.1 Hz, 2H, Ar- $\text{CHH-N}_{\text{imidazole}}$ ), 4.77 (d,  $J$  = 19.6 Hz, 2H, Ar- $\text{CHH-N}_{\text{imidazole}}$ ), 4.75 (d,  $J$  = 15.2 Hz, 2H, Py- $\text{CHH-N}_{\text{amide}}$ ), 4.60 (d,  $J$  = 15.2 Hz, 2H, Py- $\text{CHH-N}_{\text{amide}}$ ), 4.48 [s, 4H, C(O)- $\text{CH}_2\text{-N}_{\text{imidazole}}$ ].  $^{13}\text{C}$  NMR (101 MHz,  $[\text{D}_3]\text{acetonitrile}$ )  $\delta$  = 212.58, 208.75, 208.63, 208.65, 149.67, 139.95, 129.86, 129.16, 128.48, 125.76, 125.51, 125.15, 122.85, 56.02, 55.99, 52.41. ESI-MS found (calculated):  $[\text{M}-\text{Cl}]^+$   $m/z$  669.3 (669.21). Single crystals of  $[\text{Co}(\text{L3})_2]\text{PF}_6$  for X-ray structure determination were obtained from anion exchange, by adding a solution of the complex  $[\text{Co}(\text{L3})_2]\text{Cl}$  in acetonitrile to a boiling acetonitrile solution of  $\text{NH}_4\text{PF}_6$ .

## Acknowledgments

S. Luo gratefully acknowledges a grant from the Chinese Scholarship Council (no. 201306410011). We are grateful to Mr. J. M. M. van Brussel for mass spectrometry.

**Keywords:** Carbene ligands · Nickel · Cobalt · Electrocatalysis · Proton reduction

- [1] B. Rausch, M. D. Symes, G. Chisholm, L. Cronin, *Science* **2014**, *345*, 1326–1330.
- [2] N. Kaeffer, A. Morozan, J. Fize, E. Martinez, L. Guetaz, V. Artero, *ACS Catal.* **2016**, *6*, 3727–3737.
- [3] E. S. Rountree, D. J. Martin, B. D. McCarthy, J. L. Dempsey, *ACS Catal.* **2016**, *6*, 3326–3335.
- [4] D. L. DuBois, R. M. Bullock, *Eur. J. Inorg. Chem.* **2011**, 1017–1027.
- [5] J. P. Porcher, T. Fogeron, M. Gomez-Mingot, E. Derat, L. M. Chamoreau, Y. Li, M. Fontecave, *Angew. Chem. Int. Ed.* **2015**, *54*, 14090–14093; *Angew. Chem.* **2015**, *127*, 14296–14299.
- [6] X. W. Song, X. J. Gao, H. X. Liu, H. Chen, C. N. Chen, *Inorg. Chem. Commun.* **2016**, *70*, 1–3.
- [7] K. Hou, H. T. Poh, W. Y. Fan, *Chem. Commun.* **2014**, *50*, 6630–6632.
- [8] P. Zhang, M. Wang, Y. Yang, T. Yao, L. Sun, *Angew. Chem. Int. Ed.* **2014**, *53*, 13803–13807; *Angew. Chem.* **2014**, *126*, 14023–14027.
- [9] J. Berding, M. Lutz, A. L. Spek, E. Bouwman, *Organometallics* **2009**, *28*, 1845–1854.
- [10] J. Berding, T. F. van Dijkman, M. Lutz, A. L. Spek, E. Bouwman, *Dalton Trans.* **2009**, 6948–6955.
- [11] Z. Xi, B. Liu, W. Chen, *J. Org. Chem.* **2008**, *73*, 3954–3957.
- [12] M. C. Jahnke, T. Pape, F. E. Hahn, *Eur. J. Inorg. Chem.* **2009**, 1960–1969.
- [13] K. Kawano, K. Yamauchi, K. Sakai, *Chem. Commun.* **2014**, *50*, 9872–9875.
- [14] S. Luo, D. F. Bruggeman, M. A. Siegler, E. Bouwman, *Inorg. Chim. Acta* **2018**, *477*, 24–30.
- [15] S. Luo, M. A. Siegler, E. Bouwman, *Eur. J. Inorg. Chem.* **2016**, 4693–4700.
- [16] S. Luo, M. A. Siegler, E. Bouwman, *Organometallics* **2018**, *37*, 740–747.
- [17] M. van der Meer, E. Glais, I. Siewert, B. Sarkar, *Angew. Chem. Int. Ed.* **2015**, *54*, 13792–13795; *Angew. Chem.* **2015**, *127*, 13997–14000.
- [18] J.-Y. Lee, J.-Y. Lee, Y.-Y. Chang, C.-H. Hu, N. M. Wang, H. M. Lee, *Organometallics* **2015**, *34*, 4359–4368.
- [19] L. Yang, D. R. Powell, R. P. Houser, *Dalton Trans.* **2007**, 955–964.
- [20] P. Comba, W. Goll, B. Nuber, K. Várnagy, *Eur. J. Inorg. Chem.* **1998**, 1998, 2041–2049.
- [21] N. W. Alcock, G. Clarkson, P. B. Glover, G. A. Lawrance, P. Moore, M. Napitupulu, *Dalton Trans.* **2005**, 518–527.
- [22] F. A. Chavez, M. M. Olmstead, P. K. Mascharak, *Inorg. Chem.* **1996**, *35*, 1410–1412.
- [23] Z. Xi, B. Liu, C. Lu, W. Chen, *Dalton Trans.* **2009**, 7008–7014.
- [24] Z. Mo, Y. Li, H. K. Lee, L. Deng, *Organometallics* **2011**, *30*, 4687–4694.
- [25] F. Hering, J. H. J. Berthel, K. Lubitz, U. S. D. Paul, H. Schneider, M. Härterich, U. Radius, *Organometallics* **2016**, *35*, 2806–2821.
- [26] A. Massard, P. Braunstein, A. A. Danopoulos, S. Choua, P. Rabu, *Organometallics* **2015**, *34*, 2429–2438.
- [27] S. Dürr, D. Ertler, U. Radius, *Inorg. Chem.* **2012**, *51*, 3904–3909.
- [28] S. Saha, M. Kaur, K. Singh, J. K. Bera, *J. Organomet. Chem.* **2016**, *812*, 87–94.
- [29] V. Fourmond, S. Canaguier, B. Golly, M. J. Field, M. Fontecave, V. Artero, *Energy Environ. Sci.* **2011**, *4*, 2417–2427.
- [30] R. S. Nicholson, I. Shain, *Anal. Chem.* **1964**, *36*, 706–723.
- [31] M. P. Stewart, M.-H. Ho, S. Wiese, M. L. Lindstrom, C. E. Thogerson, S. Raugi, R. M. Bullock, M. L. Helm, *J. Am. Chem. Soc.* **2013**, *135*, 6033–6046.
- [32] E. S. Rountree, B. D. McCarthy, T. T. Eisenhart, J. L. Dempsey, *Inorg. Chem.* **2014**, *53*, 9983–10002.
- [33] L. Gan, T. L. Groy, P. Tarakeshwar, S. K. S. Mazinani, J. Shearer, V. Mujica, A. K. Jones, *J. Am. Chem. Soc.* **2015**, *137*, 1109–1115.
- [34] R. Tatematsu, T. Inomata, T. Ozawa, H. Masuda, *Angew. Chem. Int. Ed.* **2016**, *55*, 5247–5250; *Angew. Chem.* **2016**, *128*, 5333–5336.
- [35] E. I. Musina, V. V. Khrizanforova, I. D. Strel'nik, M. I. Valitov, Y. S. Spiridonova, D. B. Krivolapov, I. A. Litvinov, M. K. Kadirov, P. Loncke, E. Hey-Hawkins, Y. H. Budnikova, A. A. Karasik, O. G. Sinyashin, *Chem. Eur. J.* **2014**, *20*, 3169–3182.
- [36] R. M. Stolley, J. M. Darmon, M. L. Helm, *Chem. Commun.* **2014**, *50*, 3681–3684.
- [37] V. Fourmond, P.-A. Jacques, M. Fontecave, V. Artero, *Inorg. Chem.* **2010**, *49*, 10338–10347.
- [38] P. F. Huo, C. Uyeda, J. D. Goodpaster, J. C. Peters, T. F. Miller, *ACS Catal.* **2016**, *6*, 6114–6123.
- [39] R. M. Bullock, A. M. Appel, M. L. Helm, *Chem. Commun.* **2014**, *50*, 3125–3143.
- [40] P. Zhang, M. Wang, Y. Yang, D. Zheng, K. Han, L. Sun, *Chem. Commun.* **2014**, *50*, 14153–14156.
- [41] A. Kermagoret, P. Braunstein, *Organometallics* **2008**, *27*, 88–99.
- [42] M. Woods, A. D. Sherry, *Inorg. Chem.* **2003**, *42*, 4401–4408.
- [43] J. Dinda, S. D. Adhikary, S. K. Seth, A. Mahapatra, *New J. Chem.* **2013**, *37*, 431–438.
- [44] G. M. Sheldrick, *Acta Crystallogr., Sect. C Struct. Chem.* **2015**, *71*, 3–8.

Received: September 18, 2018